NASA/TM—2018-219966

Evaluation of Inflow Turbulence Methods in Large-Eddy Simulations of a Supersonic Boundary Layer

Mina R. Mankbadi, Manan A. Vyas, James R. DeBonis, and Nicholas J. Georgiadis
Glenn Research Center, Cleveland, Ohio

August 2018

NASA STI Program . . . in Profile

Since its founding, NASA has been dedicated to the advancement of aeronautics and space science. The NASA Scientific and Technical Information (STI) Program plays a key part in helping NASA maintain this important role.

The NASA STI Program operates under the auspices of the Agency Chief Information Officer. It collects, organizes, provides for archiving, and disseminates NASA's STI. The NASA STI Program provides access to the NASA Technical Report Server—Registered (NTRS Reg) and NASA Technical Report Server—Public (NTRS) thus providing one of the largest collections of aeronautical and space science STI in the world. Results are published in both non-NASA channels and by NASA in the NASA STI Report Series, which includes the following report types:

- TECHNICAL PUBLICATION. Reports of completed research or a major significant phase of research that present the results of NASA programs and include extensive data or theoretical analysis. Includes compilations of significant scientific and technical data and information deemed to be of continuing reference value. NASA counter-part of peer-reviewed formal professional papers, but has less stringent limitations on manuscript length and extent of graphic presentations.

- TECHNICAL MEMORANDUM. Scientific and technical findings that are preliminary or of specialized interest, e.g., "quick-release" reports, working papers, and bibliographies that contain minimal annotation. Does not contain extensive analysis.

- CONTRACTOR REPORT. Scientific and technical findings by NASA-sponsored contractors and grantees.

- CONFERENCE PUBLICATION. Collected papers from scientific and technical conferences, symposia, seminars, or other meetings sponsored or co-sponsored by NASA.

- SPECIAL PUBLICATION. Scientific, technical, or historical information from NASA programs, projects, and missions, often concerned with subjects having substantial public interest.

- TECHNICAL TRANSLATION. English-language translations of foreign scientific and technical material pertinent to NASA's mission.

For more information about the NASA STI program, see the following:

- Access the NASA STI program home page at http://www.sti.nasa.gov

- E-mail your question to help@sti.nasa.gov

- Fax your question to the NASA STI Information Desk at 757-864-6500

- Telephone the NASA STI Information Desk at 757-864-9658

- Write to:
  NASA STI Program
  Mail Stop 148
  NASA Langley Research Center
  Hampton, VA 23681-2199

NASA/TM—2018-219966

Evaluation of Inflow Turbulence Methods in Large-Eddy Simulations of a Supersonic Boundary Layer

Mina R. Mankbadi, Manan A. Vyas, James R. DeBonis, and Nicholas J. Georgiadis
Glenn Research Center, Cleveland, Ohio

National Aeronautics and
Space Administration

Glenn Research Center
Cleveland, Ohio 44135

August 2018

Acknowledgments

This work is supported by NASA's Transformational Tools and Technology (TTT) project. Computational resources were provided by the NASA High-End Computing (HEC) program through the NASA Advanced Supercomputing (NAS) Division at Ames Research Center.

This work was sponsored by the
Transformative Aeronautics Concepts Program.

Level of Review: This material has been technically reviewed by technical management.

Available from

NASA STI Program
Mail Stop 148
NASA Langley Research Center
Hampton, VA 23681-2199

National Technical Information Service
5285 Port Royal Road
Springfield, VA 22161
703-605-6000

This report is available in electronic form at http://www.sti.nasa.gov/ and http://ntrs.nasa.gov/

Evaluation of Inflow Turbulence Methods in Large-Eddy Simulations of a Supersonic Boundary Layer

Mina R. Mankbadi, Manan A. Vyas, James R. DeBonis, and Nicholas J. Georgiadis
National Aeronautics and Space Administration
Glenn Research Center
Cleveland, Ohio 44135

Abstract

Wall-resolved Large-eddy simulations (LES) were used to investigate inflow turbulence of a supersonic boundary layer. Two high-order structured Navier-Stokes solvers were used to calculate a Mach 2.29 boundary layer at $Re_\theta = 4{,}640$. The purpose of this work is to evaluate and compare two different synthetic inflow turbulence methodologies through careful examination of the Reynolds stress tensor, skin friction coefficient, and adjustment length. Boundary-layer inflow turbulence was simulated using both the Synthetic Eddy Method (SEM) and Digital Filtering (DF). The LES results showed that both methods reasonably account for the effects of inflow turbulence. They demonstrated good agreement with experimental data for the mean and fluctuating velocities. In particular for SEM, a length scale of $\delta/5$ matched the experimental skin friction coefficient. Whereas, very small length scales such as $\delta/10$ or $\delta/20$ attenuated the overall turbulence levels. In particular for DF, the implementation was compared between two flow solvers. Although the Reynolds tensor profiles compared well with experiment, the values of the skin-friction coefficient differed by 15 percent and were tabulated. Both DF and SEM adjustment lengths were 6δ and did not significantly differ between simulations.

Nomenclature

C_f	skin friction coefficient
E	total energy per unit mass
f	frequency
k	turbulent kinetic energy
κ	wave number
L	SEM length scale
M	freestream Mach number
N	number of eddies
P	pressure
q_i	heat flux
Re	Reynolds number
T	temperature
t	time
U	mean velocity
u_i	Favre-filtered velocity
u_τ	friction velocity
u^+	dimensionless mean velocity
$\overline{u_i'u_j'}/u_\tau^2$	dimensionless Reynolds streamwise normal stress
x_i	Cartesian coordinate
y^+	wall coordinate

τ_{ij}	stress tensor
ρ	density
δ^*	displacement thickness
δ	boundary layer thickness
Θ	momentum thickness

Subscripts:

0	total condition
w	wall properties
∞	freestream properties
i	index
j	index

Superscripts:

+	wall coordinates
$'$	fluctuating

1.0 Introduction

In recent years, there has been interest in accounting for the effects of inflow turbulence when performing high-fidelity computational fluid dynamics simulations, such as those described in Klein et al., (Ref. 1) Lund et al., (Ref. 2) and DiMare et al. (Ref. 3). This was prompted by awareness of the need for unsteady inflow boundary conditions in order to obtain an accurate scale-resolving solution. It is well known that simulating natural transition in LES is computationally impractical due to the large computational costs. Neither does artificial tripping address this need, since it produces mixed results that are imprecise and arbitrary (Ref. 1). Recycling and rescaling, proposed by Lund et al. (Ref. 2), was the first practical solution. But, it requires an ancillary LES known to be computationally expensive. This work is motivated by the need for a less-expensive and more user-friendly turbulent inflow technique. The purpose of this work is to evaluate and compare two different synthetic inflow turbulence methodologies through careful examination of the Reynolds stress tensor, skin friction coefficient, and adjustment length.

Specifying unsteady turbulence at inflow boundaries is an active area of research (Refs. 1 to 13). Various methods over the past two decades have been presented to the community with differing degrees of cost, accuracy, and complexity. The simplest inflow turbulence methodology imposes random fluctuations that are limited by amplitude to satisfy a given Reynolds stress tensor. Although it is cost-effective, it often fails to produce sustained turbulence (Refs. 6 and 7). The turbulent kinetic energy is distributed equally across all frequencies. This is contrary to real turbulence where low frequency turbulence (large length scales) have more energy than high frequency turbulence (small length scales). Consequently, the turbulence from this method is not consistently correlated and decays rapidly after the inflow plane due to the absence of large length scale turbulence (Ref. 7).

The recycling and rescaling method uses an auxiliary boundary layer simulation and boundary layer scaling laws to generate the inflow profile (Ref. 2). To reduce the cost of the auxiliary simulation, the outflow profile is recycled by rescaling it to the inflow conditions. There are two limitations to this method, firstly, a spurious low frequency mode is introduced based on the distance between the recycling station and inflow plane (Refs. 8 and 9). Secondly, the boundary layer scaling laws require an equilibrium region. The high computational cost and possible contamination of the solution with low frequency modes inspired a class of *synthetic turbulence* methods. In turbulence, most of the energy is contained in

the large scales and then energy is transferred to smaller scales via a cascade. Some synthetic turbulence methods attempt to mimic this energy-exchange mechanism (Ref. 13).

This work will evaluate in particular the synthetic turbulence methods of Synthetic Eddy Method (SEM) and Digital Filtering (DF) (Refs. 1 and 12). They are stochastic algorithms that generate an instantaneous velocity profile from a specified time-averaged Reynolds stresses. The assumption that synthetic turbulence methods make is that a turbulent flow can be approximated by reproducing a set of low-order statistics such as mean velocities and Reynolds stresses. The artificially generated structures obtained from SEM or DF do not necessarily satisfy the Favre-fitered Navier-Stokes equations being solved in an LES. Consequently, these methods require a redevelopment or *adjustment* region. An elongated adjustment region has an added computational cost that may be comparable to the rescaling/rescaling method, hence it is worth investigating this adjustment region.

This work uses the test problem of a supersonic boundary layer to assess the effectiveness of synthetic turbulence methods. The experiments of Dussauge et al. (Ref. 14) were used for validation and as a measure of the effectiveness of: (1) Synthetic Eddy Method; and (2) Digital Filtering. The length of the adjustment region necessary for synthetic inlet turbulence to recover from modelling errors will be estimated herein. The effect of varying the integral length scales of the turbulent fluctuations will be studied and recommendations will be made for choosing these parameters. Both SEM and DF inflow turbulence methodologies are evaluated within the Wave-Resolving LES (WRLES) code, henceforth referred to as WRLES-SEM and WRLES-DF. Another flow solver FDL3DI is used to establish confidence in the robustness of DF with respect to numerical scheme, henceforth referred to as FDL3DI-DF.

This paper is organized as follows. Section 1.0 gives a quick overview of the governing equations of Implicit LES and synthetic turbulence methodologies. Section 2.0 describes the supersonic boundary layer and experiment. Section 3.0 describes the flow solvers, boundary conditions, and wall-resolved grid. The results of this work presented in Section 5.1 will examine the effect of the SEM length scale on the Reynolds stresses, skin friction coefficient, and adjustment length. Section 5.2 will be a comparison of SEM and DF inside the WRLES code. Section 5.3 will compare the DF implementation across two LES solvers to establish confidence in our results.

2.0 Formulation

2.1 Navier-Stokes

In Large eddy simulations (LES), large-scale structures are resolved and a subgrid scale model is used to represent the scales that cannot be captured due to insufficient grid. Implicit LES (ILES) calculates the large-scale structures but does not use a subgrid scale model. Instead, the numerical dissipation present in the simulation, serves as the sub-grid closure. Since the numerical dissipation scales with the grid size, ILES provides a seamless transition to DNS as the grid is refined. All of the work herein uses the ILES approach. The Navier-Stokes equations are solved while the viscosity and thermal conductivity are allowed to vary with temperature. The continuity, momentum, and energy equations are:

$$\frac{\partial \rho}{\partial t} + \frac{\partial}{\partial x_i}(\rho u_i) = 0, \tag{1}$$

$$\frac{\partial (\rho u_i)}{\partial t} + \frac{\partial}{\partial x_j}\left(\rho u_i u_j\right) + \frac{\partial P}{\partial x_i} = \frac{\partial \tau_{ij}}{\partial x_j}, \tag{2}$$

$$\frac{\partial E}{\partial t} + \frac{\partial}{\partial x_j}\left(u_j E + u_j P\right) = \frac{\partial}{\partial x_j}\left(u_i \tau_{ij}\right) + \frac{\partial q_j}{\partial x_j}. \tag{3}$$

The velocity is denoted as u_i, while the density and pressure are ρ and P, respectively. The viscous stress tensor is τ_{ij}. The effect of the numerical filter on the flow solution was explored in a previous study (Refs. 4 and 5).

2.2 The Synthetic Eddy Method (SEM)

The Synthetic Eddy Method (SEM) by Jarrin et al. (Refs. 12 and 13) is applied to the boundary layer under consideration to simulate the effects of inflow turbulence. It requires four inputs: (1) a Reynolds stress tensor, (2) the mean flow, (3) a turbulent length scale, and (4) a convective velocity. The SEM method represents the turbulent flow field as a collection of eddies, and convects these eddies through a box around the inflow plane. Each individual eddy has a contribution to the instantaneous velocity component at a given point, based on its distance from that point and the turbulent length scale. This ensures that fluctuations being added to the mean flow are correlated. The instantaneous component is then added to the mean flow to obtain the total instantaneous velocity. SEM scales the velocity fluctuations according to the Reynolds stress tensor in such a way, that when the flow is time-averaged, the original Reynolds stress tensor is retrieved at the inflow plane. A detailed formulation can be found in Reference 12.

The original work of Jarrin et al. (Refs. 12 and 13) does not cover compressible cases where the temperature and density profile are varying within the boundary layer. For this work, the mean density and pressure profiles were specified at the SEM inflow boundaries based on the precursor RANS simulation. No fluctuating pressure or density signal was added to the Reynolds averaged mean values of pressure and density. The method appeared to be sensitive to the length scale especially when the length scale was too large (Refs. 4 and 5). In these instances, it failed to replicate the Reynolds stress tensor at both the inflow plane and downstream stations. The original formulation adjusted the length scale in regions where the grid was too coarse. Here, the length scale was not adjusted based on the maximum grid size, instead it was best to ensure that the grid was fine enough to resolve the specified length scale. The convective velocity was set to half of the freestream value, $U_{conv} = U_{\infty}/2$.

2.3 Digital Filtering (DF)

The Digital Filtering (DF) method was originally proposed by Klein et al. (Ref. 1). The DF method is applied to the boundary layer under consideration to simulate the effects of inflow turbulence. It requires four inputs: (1) a Reynolds stress tensor, (2) the mean flow, and (3) a turbulent length scale in each direction, and (4) a convective velocity. In DF, a filter with a width corresponding to the specified length scale is applied to a set of random numbers distributed on the inflow plane. The filtering process provides structure to the random signal, which serves as the artificially generated turbulent structure. This signal is scaled by the input Reynolds stresses to obtain the instantaneous velocity components, that when averaged provide the specified Reynolds stresses. The data at the current time step is correlated with previous time steps using a time correlation function. Originally, a Gaussian two-point correlation function was used.

The implementation herein follows the work of Xie and Castro (Ref. 11). The original method employed 3D random data and filtering, whereas, the method of Xie et al. (Ref. 11) requires only 2D filtering operations on the inflow plane. In addition, an exponential correlation function rather than a Gaussian is used to advance the solution in time. A further modification is made in this work. Here, the filtering process is performed on the computational grid, rather than a uniform grid, avoiding the need for interpolation onto the computational grid. The filter width is scaled with the local grid size in order to produce the correct length scale. The mean density and pressure profiles were specified, based on the precursor RANS simulation. No fluctuating pressure or density signal was added to the Reynolds averaged mean values of pressure and density. The integral length scale of the filter chosen was 1/2 of the boundary layer height in all three directions. More details about the 2D implementation are provided in Vyas et al. (Ref. 15).

TABLE 1.—FLOW CONDITIONS

Parameter	Value
M_∞	2.29
$U_\infty, m/s$	545.0
P_∞, Pa	50663
T_0, K	300
δ_{99}, mm	10.0
Θ, mm	0.87
δ^*, mm	3.0
Re_δ	53,420
Re_θ	4,640
C_f	2.1E-3

3.0 Boundary-Layer Description

The boundary layer simulated here corresponds to the experiments of Dussauge et al., (Ref. 14) which were carried out in the turbulent supersonic wind tunnel at the *Institut Universitaire des Systemes Thermiques Industriels* (IUSTI). Table 1 shows the experimental flow conditions used for the LES. Since the Reynolds number is moderate at 53,420, we were able to match it without exhausting numerical resources. A precursor 2D RANS simulation was used to develop a boundary layer thickness of 10 mm matching these operating conditions. The resulting Reynolds stress tensor and mean flow profiles were used as inputs for the synthetic turbulence methodologies under examination. The experimentalists gathered Reynolds stress information at their $x = 280\ mm$ station which corresponds to the LES station of $x/\delta = 10$. Mean flow and stress profiles are compared with the experimental PIV data for validation purposes.

4.0 Computations

4.1 Flow Solver: WRLES

Both the Synthetic Eddy Method and Digital Filtering are built into the high-order Wave-Resolving LES (WRLES) code (Refs. 16 and 17) SEM and DF are compared within the same framework to ensure a consistent and fair assessment. WRLES is a finite difference code which contains central-differencing schemes that employ up to 13 point stencils. A Dispersion Relation Preserving (DRP) scheme developed by Bogey & Bailly (Ref. 18) was used here. The stencil size is 11 points and is formally fourth-order accurate. While a traditional fourth-order scheme uses fewer points in the stencil, the additional points in the DRP scheme are used to minimize the dispersion error. It is an explicit central scheme similar to the classic tenth-order central scheme but with weights carefully chosen to minimize the dispersion error. Since it is a central differencing scheme, it is not inherently dissipative. A spatial filter, developed specifically to match the resolution of the differencing scheme, is used to preserve numerical stability. A coefficient multiplying the effect of the filter has been added, so that the magnitude of the dissipation can be controlled. The DRP filter coefficient used was 0.5. Temporal discretization is performed using a low-dissipation and low-dispersion forth-order Runge-Kutta algorithm summarized in Berland et al. (Ref. 19).

WRLES uses the Message Passing Interface (MPI) standard to divide the domain across nodes and the Open Multi-Processing (OpenMP) directive to parallelize work across the cores on each node. In order to maintain order accuracy across interfaces, WRLES uses a 10-point overlapping, point-matched zone coupling.

4.2 Flow Solver: FDL3DI

Only digital filtering was investigated within the FDL3DI code (Rizzetta et al., (Ref. 20) Visbal & Gaitonde, (Ref. 21) Visbal & Rizzetta (Ref. 22). FDL3DI is a finite difference code that employs a compact scheme to discretize the spatial derivatives in the governing equations. For the present computation, the viscous fluxes are computed using the 6th order compact scheme. Near the boundaries the order of the scheme is reduced to fourth order compact. The time marching is accomplished by incorporating the second-order accurate backward-implicit method of Beam and Warming (Ref. 20). An 8th order Pade-type filer is used for filtering, that requires a 9-point stencil. It is a nondispersive spatial filter and has been shown to be superior to the use of artificial dissipation. FDL3DI also uses the parallel MPI standard. The order is preserved across blocks through the utilization of an 11-point overlap.

4.3 Boundary Conditions

The boundary condition (BC) imposed on the top-wall is a nonreflecting characteristic freestream that allows shocks to leave the domain. On the inflow plane, digital filtering is applied for the entire extent of the transverse domain, whereas SEM is applied up to $y/\delta \sim 1.2$. After which a supersonic inflow boundary condition specifying the Mach number, pressure, and temperature is used. Both flow solvers use a supersonic outflow boundary condition that extrapolates values from the interior. An adiabatic viscous wall boundary condition was used. A periodic boundary condition was applied in the spanwise-direction for all simulations.

4.4 Grid

The grid was kept fixed for both flow solvers and inflow turbulence methodologies. Grid details such as the number of points, wall spacing, domain size, and minimum/maximum grid spacing are provided in Table 2. The grid used is structured as shown in Figure 1. The coordinates are nondimensionalized by the boundary layer height, δ. The width of the spanwise domain was 5δ with uniform spacing. The total length of the section is 30δ with grid-stretching at 20δ towards the outflow boundary condition. The mesh uses 67.7 million points to resolve the boundary layer. The smallest grid spacing in the wall normal direction corresponds to a y^+ value of 0.7 to ensure that the viscous sub-layer is resolved. About 187 points in y were used within the boundary layer itself.

TABLE 2.—GRID PROPERTIES OF THE BOUNDARY LAYER MESH

Parameter	Grid[a]		
	x	y	z
Number of points	1025	257	257
Wall spacing ($\Delta x^+, \Delta y^+ \Delta z^+$)	15	0.68	13
Length of domain	30	4	5
Minimum spacing	0.021	0.001	0.0195
Maximum spacing after $x/\delta = 20$	0.465	0.078	0.0195

[a]Nondimensionalized by δ

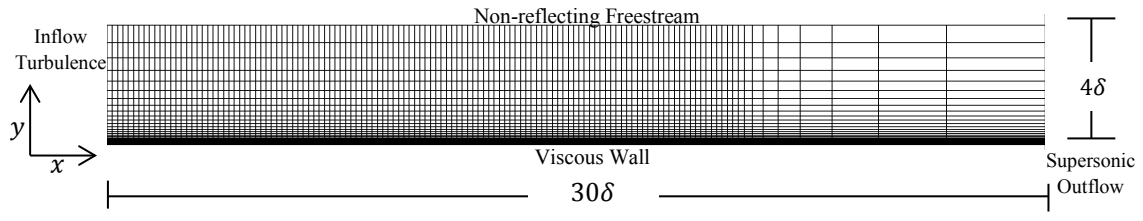

Figure 1.—Boundary conditions and dimensions of the LES supersonic boundary layer simulation (only every 8th point is plotted).

5.0 Results

Three sub-sections of results will be presented: (a) The effect of the SEM length scale on the boundary layer will be investigated. (b) Compares the Synthetic Eddy Method to Digital Filtering within the same code. (c) A code-to-code comparison of digital filtering will be conducted. LES best practices such as time-averaging and spanwise-averaging described in Georgiadis et al. (Refs. 24 and 25) were implemented herein. The solution was initialized to freestream conditions, then run for 30 flow-through periods to allow the inflow turbulence boundary condition to establish a turbulent boundary layer. After which data for time-averaging was gathered for 15 flow-through periods. Turbulent statistics were collected over the entire domain, after which they were spanwise averaged. Both FDL3DI and WRLES used the ILES approach. A precursor RANS was used as an input for SEM and DF.

5.1 SEM Length Scale Study: WRLES-SEM

The purpose of this subsection is to assess the effect of the SEM length scale on the streamwise velocity, Reynolds stresses, and adjustment length. All of these simulations are done in the WRLES-SEM framework. Three length scales, $L = \delta/5, \delta/10, \delta/20$, were examined. For the length scale of $L = \delta/5$, Figure 2 depicts the mean velocity profiles in wall scaled coordinates. The flow adjusts from the artificial structures imposed at the boundary to realistic structures supported by the LES equations. The variation in the boundary layer profiles are caused by the variations in the local friction velocity. As the flow moves downstream from $x/\delta = 0$ to 4 the scaled boundary layer edge velocity (u^+_{max}) adjusts from 24 to 22. All of the profiles downstream of $x/\delta = 4$ are no longer changing significantly and are a good match with the experimental data in both the outer and inner portions of the boundary layer.

Figure 3 depicts a similar trend for the Reynolds stress profiles at downstream stations x/δ= 2, 4, 6, 8, 10, and 12. In Figure 3(b) to (d), the normal stresses at $x/\delta = 0$ peak at 3.2. These values come from the 2D precursor RANS simulation which does not differentiate between the normal stresses. As such, the turbulent kinetic energy is distributed equally across the streamwise (Figure 3(b)), transverse (Figure 3(c)), and spanwise stresses (Figure 3(d)). This is clearly a limitation of the RANS methodology. LES does not have this limitation since it computes these quantities directly. SEM artificially generates turbulence, and although it matches the input Reynolds tensor, it does not necessarily satisfy the Navier-Stokes equations instantaneously. Consequently, there is an adjustment region between where the peak Reynolds stress adjusts from the RANS imposed values at the inflow to satisfy the LES equations.

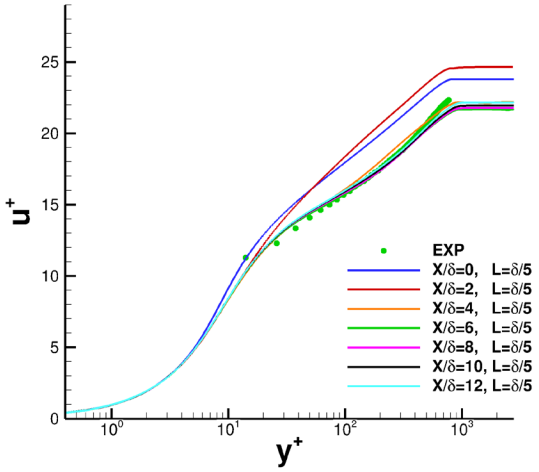

Figure 2.—Time averaged streamwise velocity for the SEM $L = \delta/5$ case.

In Figure 3(a), the Reynolds shear stress is shown to converge after $x/\delta = 6$. Figure 3(b) depicts the streamwise stress which has a well predicted peak of 8.28 at $x/\delta = 6$ that matches the experimental peak of 8.44. Figure 3(c) illustrates the transverse stress which is slightly over predicted by the simulation. Figure 3(d) depicts the spanwise stress which continuously drops with downstream axial location. Comprehensively, the flow is adjusting to the synthetic turbulence between $x/\delta = 0$ to 6.

The former length scale of $L = \delta/5$ is compared with two new simulations of length scales $L = \delta/10$ and $L = \delta/20$. The mean velocity profiles at $x/\delta = 10$ are shown in Figure 4. There is an observable difference in the boundary layer profiles. The $L = \delta/5$ case matches with experiment very well. In contrast, the $L = \delta/10$ and $L = \delta/20$ cases over predict velocity magnitude outside of the laminar sublayer.

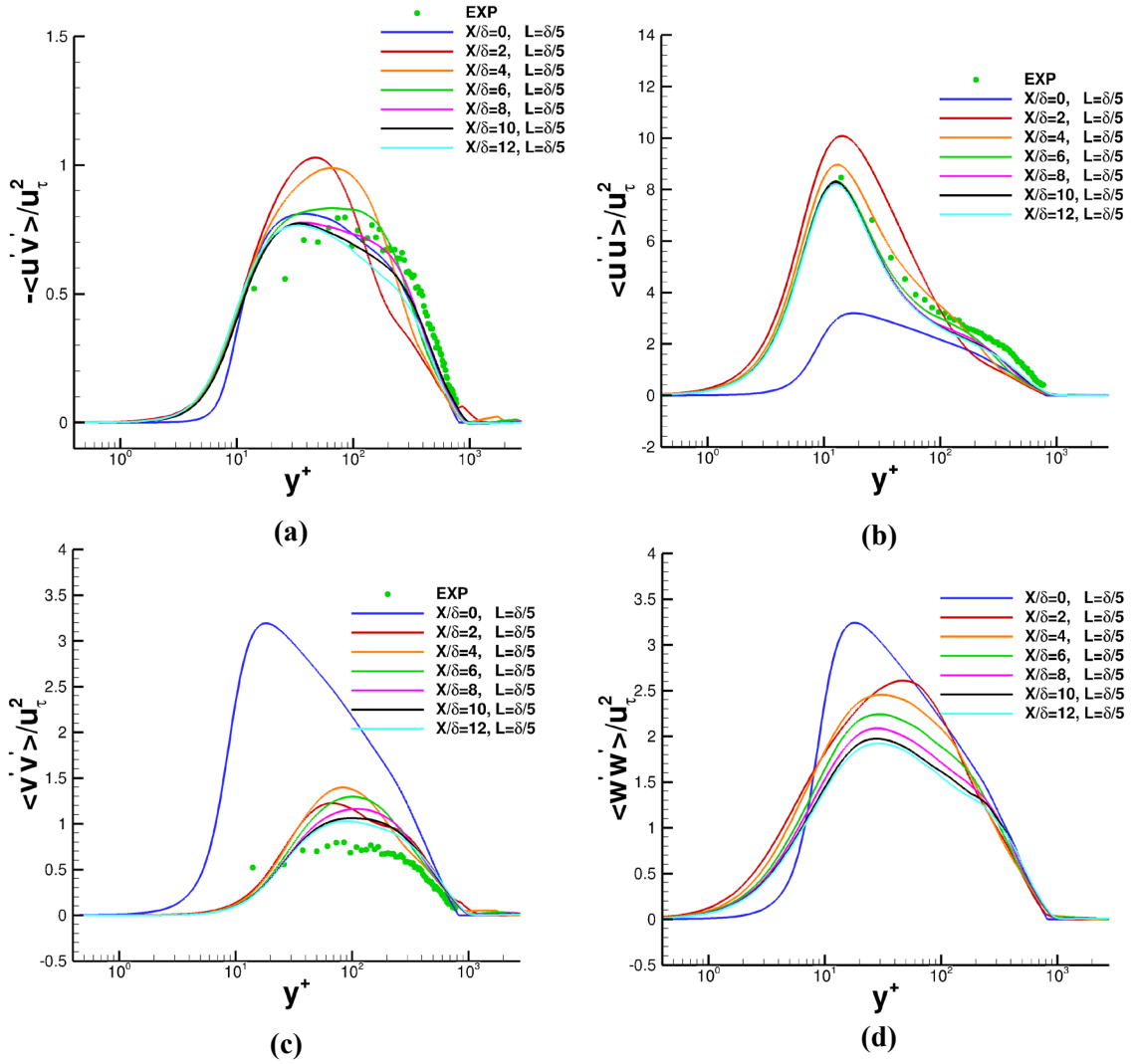

Figure 3.—Reynolds stresses: (a) shear stress; normal stresses (b) streamwise, (c) transverse, and (d) spanwise, for the SEM $L = \delta/5$ case.

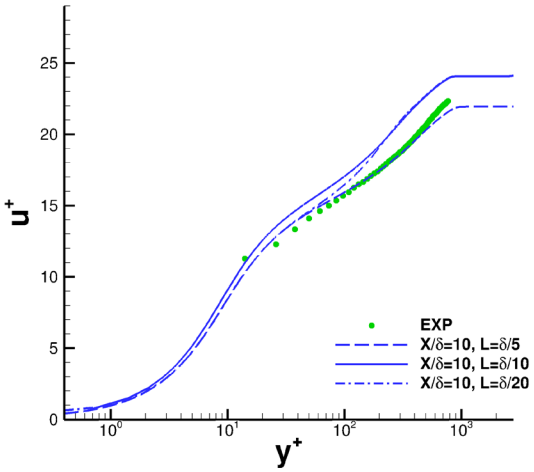

Figure 4.—Time averaged streamwise velocity for the SEM length scale study.

In Figure 5(a), the shear stress profiles at $x/\delta = 10$ are shown. The LES solution with $L = \delta/20$ under-predicts the shear stress levels in the outer portions of the boundary layer. The LES solution with $L = \delta/5$ is the closest match between simulation and experiment. The peak shear stress predictions in the outer portions of the boundary layer gradually improve as the length scale increases from $L = \delta/20$ to $L = \delta/5$. Figure 5(b) depicts the streamwise normal stress. Again the $L = \delta/5$ LES is the closest match between simulation and experiment. The experimental peak value of $\overline{u'u'}/u_\tau^2$ is 8.44, which matches closely with the 8.28 prediction of the $L = \delta/5$ simulation. Although the peak value predictions match the experiment well, the stress levels in the outer portions of the boundary layer after the peak between a $y^+$of 30-100 are slightly under-predicted. The improvement in the outer portions of the boundary layer with increasing length scale in Figure 5(a) and (b) is consistently seen in Figure 5(c) and (d). The transverse stress is shown in Figure 5(c). The peak value is not significantly affected by the length scale; however, the outer portions of the boundary layer agree best with the $L = \delta/5$ simulation. Figure 5(d) depicts the spanwise stress. Increasing the length scale from the $L = \delta/20$ to $L = \delta/10$ resulted in a noticeable increase in the peak value predicted. However, there is good saturation of the peak value between the $L = \delta/10$ and $L = \delta/5$ simulations. Note that the $L = \delta/5$ LES consistently predicts the highest turbulence values in the outer boundary layer.

The spectra of the turbulent kinetic energy are plotted in Figure 6. The data for the plots were obtained on the inflow plane at $y^+ = 12$. The location was chosen to correspond to the location of the peak shear and streamwise stresses. The spectra were computed for each point in z, then spanwise averaged. Peaks in the spectra are seen at the inflow plane ($x/\delta = 0$) beyond 200 kHz for all three cases. The first peaks in the spectra are at 272, 545, and 1087 kHz, for $L = \delta/5, \delta/10, \delta/20$ respectively. The $L = \delta/5$ and $\delta/10$ simulations contain harmonics of the primary frequency. It was theorized that these peaks represent artificial modes imposed on the flow by the SEM method. This was confirmed by computing the representative frequency of the SEM process, by using the eddy convection velocity and turbulent length scale; $f_{SEM} = U_{conv}/L$. In the SEM method, the synthetic eddies travel the distance, L, at the velocity, U_{conv}, before being replaced in the simulation. The resulting SEM induced frequencies were 272, 545, and 1090 kHz for $L = \delta/5, \delta/10, \delta/20$ respectively, confirming that these modes are artificially introduced by the SEM.

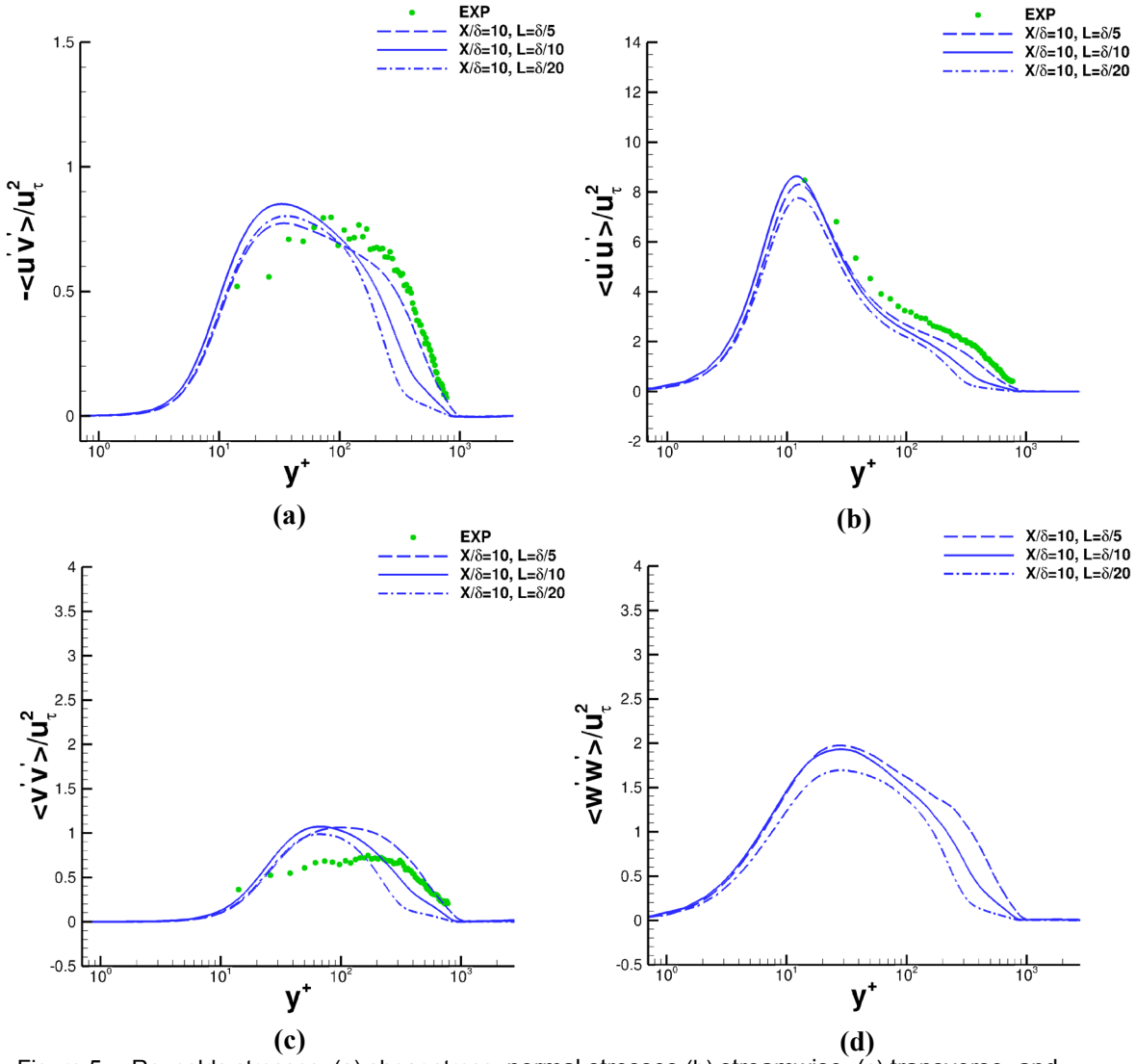

Figure 5.—Reynolds stresses: (a) shear stress; normal stresses (b) streamwise, (c) transverse, and (d) spanwise, for the SEM length scale study.

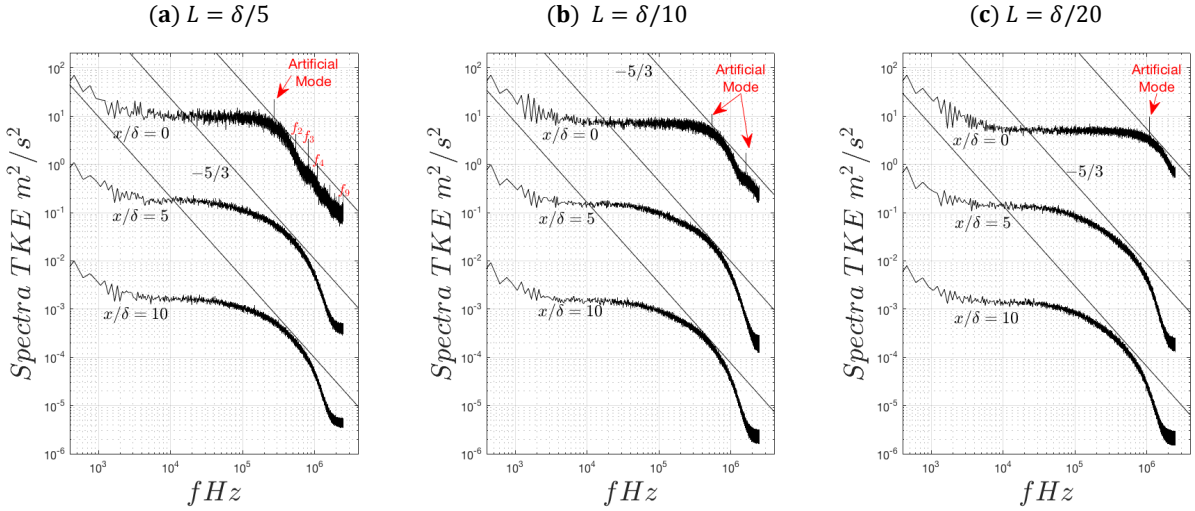

Figure 6.—Energy spectra for the SEM length scale study, shifted down by two orders of magnitude.

The spectra show that the distribution of energy at the inflow plane is clearly related to the length scale specified. The larger the length scale, the more energy in the lower frequencies. As the length scale decreases more energy is placed at the higher frequencies. This can explain the reduction in the peak Reynolds stresses with decreasing length scale, because the simulation dissipates the energy at the highest frequencies. This is further seen in Figure 7 where the $\delta/20$ simulation contains the least energy. The downstream spectra show that the energy is redistributed to satisfy the LES equations and at $x/\delta = 10$, the three simulations show very similar energy distributions. The downstream spectra also show that the artificial modes have been eliminated.

In Figure 8, the axial evolution of skin friction coefficient for all three length scales is shown. It is interesting to note that the C_f value of the $L = \delta/10$ and $L = \delta/20$ are the same, whereas the $L = \delta/5$ simulation is higher by about fifteen percent. Recall the experimental C_f value is 2.10E-3, it matches closely the value of 2.16E-3 predicted by the $L = \delta/5$ LES (Table 3). In contrast, the simulations with $L = \delta/10$ and $L = \delta/20$ both predict a C_f value of 1.80E-3, a 15 percent difference from experiment. Figure 9 depicts the derivative of the skin friction coefficient (dC_f/dx), which is a metric used to discern the extent of the adjustment region. The slope between $x/\delta = 0$ and 6 varies significantly in the plot, hence the flow is adjusting within this region. However, it flat lines to be an infinitesimal negative number between $x/\delta = 6$ to 12. Consequently, the adjustment length for all three SEM length scales is 6δ based upon the mean flow profiles, Reynolds stress profiles, skin friction coefficient, and as clearly seen by dC_f/dx. Hence forth this comprehensive methodology is used to discern the length of the adjustment region objectively.

The key findings of this subsection are that although the choice of length scale did not adversely affect the adjustment length, it had a noticeable effect on the Reynolds stress profiles. Increasing the length scale from $L = \delta/20$ to $L = \delta/5$ improved the prediction of C_f by 15 percent resulting in a good match with the experimental value of 2.10E-3. The choice of length scale of $L = \delta/5$ resulted in a closer Reynolds stress profile match to experiment.

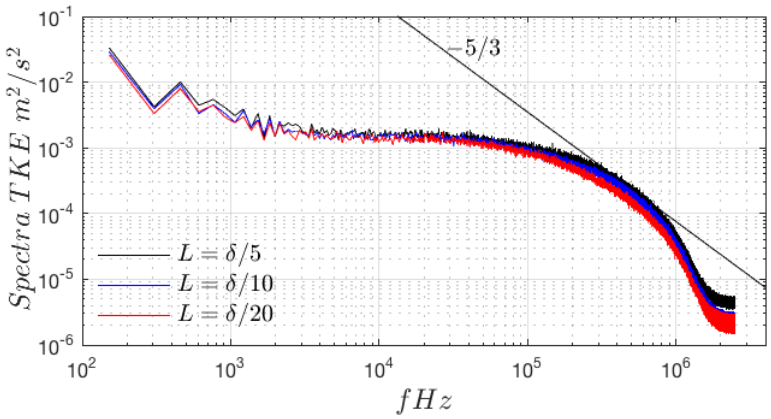

Figure 7.—Comparison of Energy spectra at $x/\delta = 10$ for the SEM length scale study.

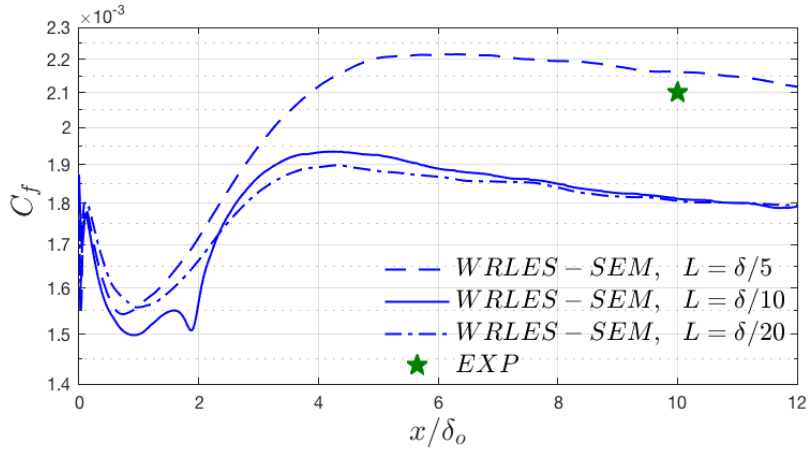

Figure 8.—Skin friction coefficient for the SEM length scale study.

TABLE 3.—SKIN FRICTION COEFFICIENT

Simulation methodology	C_f
Experiment	2.100 E-3
Input ($x/\delta = 0$)	1.845 E-3
WRLES-SEM, $L = \delta/5$	2.161 E-3
WRLES-SEM, $L = \delta/10$	1.806 E-3
WRLES-SEM, $L = \delta/20$	1.806 E-3
WRLES-DF	1.920 E-3
FDL3DI-DF	1.880 E-3

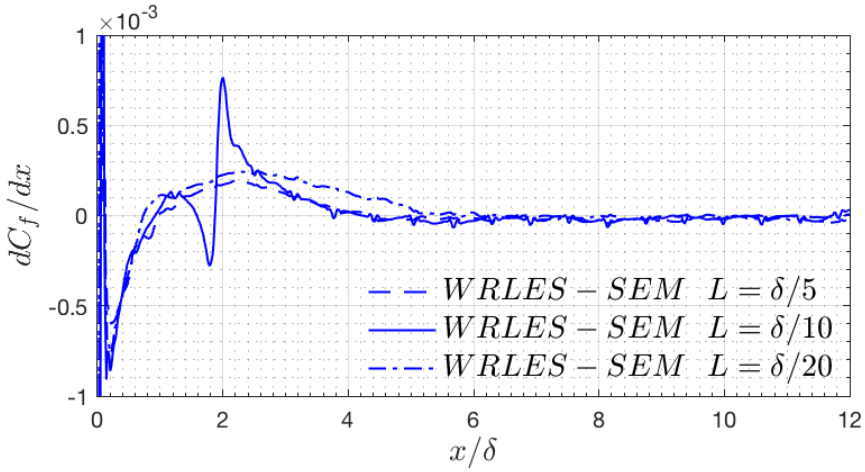

Figure 9.—Skin friction coefficient rate of change, dC_f/dx, for the SEM length scale study.

5.2 Evaluation of Inflow Turbulence Methodologies: WRLES-SEM and WLRES-DF

The purpose of this section is to compare WRLES-SEM with WRLES-DF results. The SEM length scale used is $\delta/5$. The length scale used for the DF simulation was $\delta/2$, based on previous work (Ref. 15). Figure 10 compares the supersonic boundary layer's mean flow profile both at the inflow plane ($x/\delta = 0$) and downstream at $x/\delta = 10$ for both the LES results and the experiment. Both simulations produce classic law-of-the-wall behavior. The SEM result shows good agreement with the experiment. The DF simulation over-predicts the scaled velocity (u^+), indicating that the friction velocity, and hence wall shear stress is too low.

Figure 11 depicts the Reynolds stresses at stations of $x/\delta = [0, 10]$ for both WRLES-DF and WRLES-SEM. For WRLES-DF, the normal stress peak values adjusted from the inflow's 3.2, 3.2, and 3.2 ($x/\delta = 0$) to 9.4, 1.3, and 2.6 at $x/\delta = 10$ for the streamwise, transverse, and spanwise normal stresses, respectively. Note that the inflow values of the normal turbulent stresses are the same because the RANS model is a linear two equation model with no differentiation in $\overline{u'u'}/u_\tau^2$, $\overline{v'v'}/u_\tau^2$, $\overline{w'w'}/u_\tau^2$ from k. For WRLES-SEM, the normal stress peak values adjusted from the inflow's 3.2 ($x/\delta = 0$) in the three normal directions to 8.1, 1.1, and 2.0 at $x/\delta = 10$ for the streamwise, transverse, and spanwise normal stresses, respectively. For WRLES-DF, the shear stress peak value adjusted from about 0.75 ($x/\delta = 0$) to 0.92 ($x/\delta = 10$). For WRLES-SEM, the shear stress peak value adjusted from about 0.81 ($x/\delta = 0$) to 0.77 ($x/\delta = 10$). Note that the y^+ location of the peak differs between each stress component.

Overall, the Reynolds stresses are predicted reasonably well by the simulations. WRLES-DF consistently over predicts, WRLES-SEM consistently under predicts, and the experiment lies between the two. In Figure 11(a)'s shear stress at $x/\delta = 10$, the WRLES-DF solution is a closer match to the experimental data than the WRLES-SEM solution in the outer portions of the boundary layer. In contrast Figure 11(c) shows the peak transverse stress of WRLES-SEM solution is a closer match to the experimental data than the WRLES-DF solution. In Figure 11(b), there is good agreement in the peak streamwise stress predicted by simulations and the experiment. Again, we see a closer match between WRLES-DF and the experiment for the transverse stress. There is no experimental data for the spanwise stress.

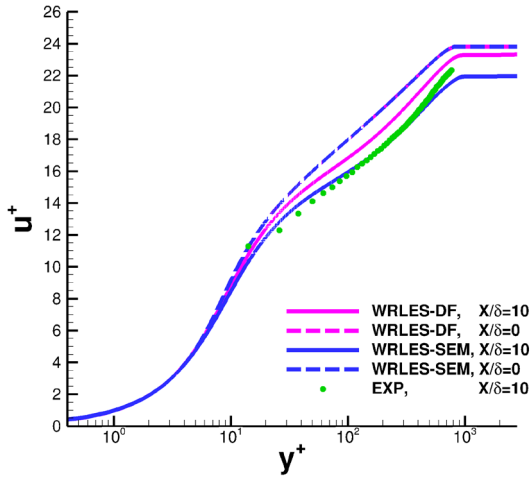

Figure 10.—Time averaged streamwise velocity for the comparison between WRLES-SEM and WRLES-DF.

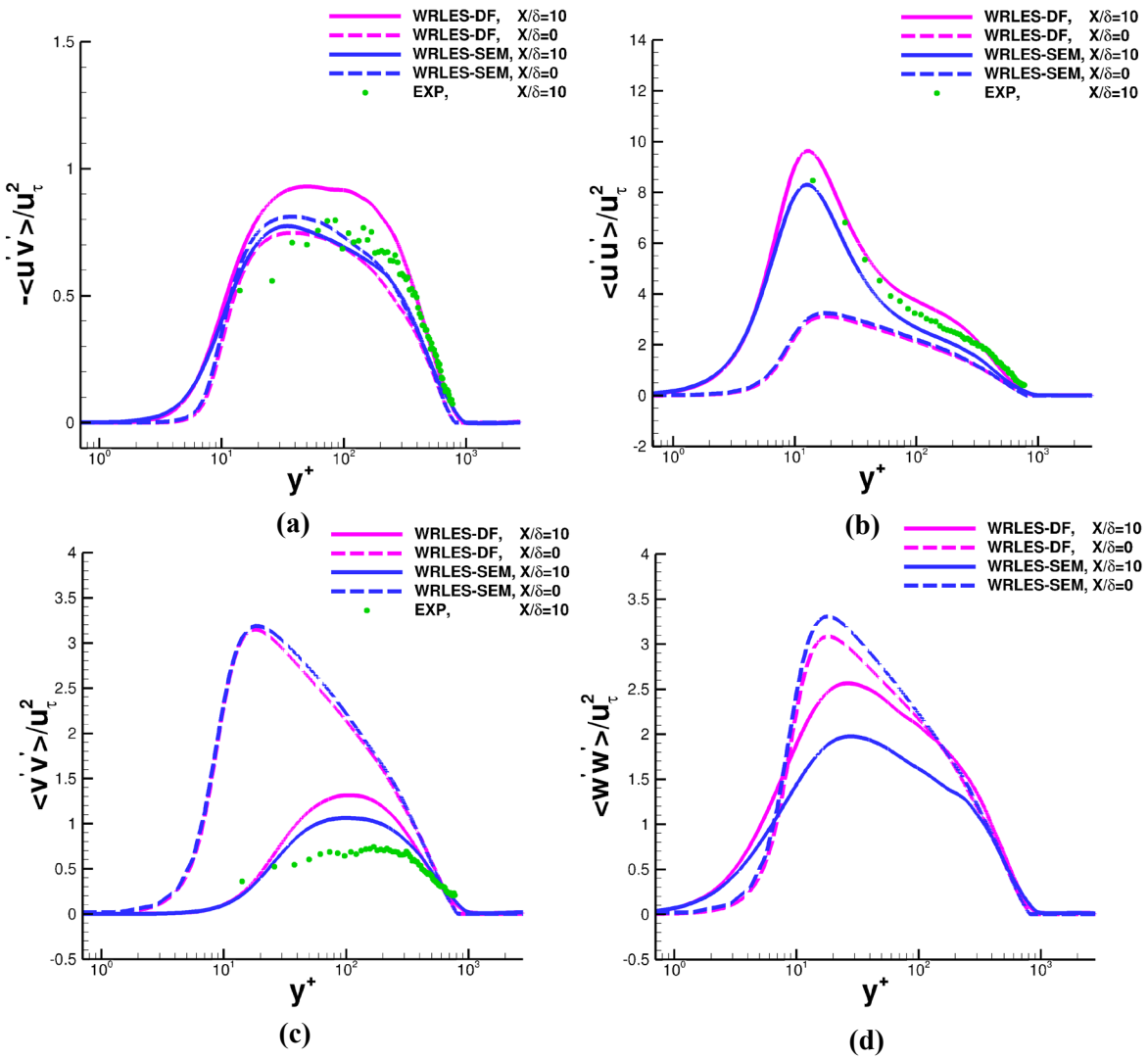

Figure 11.—Reynolds stresses: (a) shear stress; normal stresses (b) streamwise, (c) transverse, and (d) spanwise, for the comparison between WRLES-SEM and WRLES-DF.

Skin friction coefficient is plotted versus downstream distance in Figure 12. The experimental value of the skin-friction coefficient is 2.10E-3 as shown in Table 1. The value of C_f adjusts from the inflow value by dropping for several boundary layer heights before recovering. The value of C_f predicted is 1.92E-3 and 2.16E-3 for WRLES-DF and WRLES-SEM, respectively (Table 3). The adjustment length is 6δ for both WRLES-DF and WRLES-SEM based upon the mean flow, Reynolds stress profiles, skin friction coefficient, and dC_f/dx.

The key finding is that both SEM and DF produced reasonable results for the supersonic boundary layer. The impact of this sub-section means that either method can accurately replicate inflow turbulence provided the mesh is wall-resolved. Flow problems involving separation and shock-boundary layer-interactions can be simulated using SEM or DF. There was a negligible change in computational time between the two methods of about 3 percent. For SEM, the computational time required can vary slightly depending on the number of eddies used, which is controlled by the length scale.

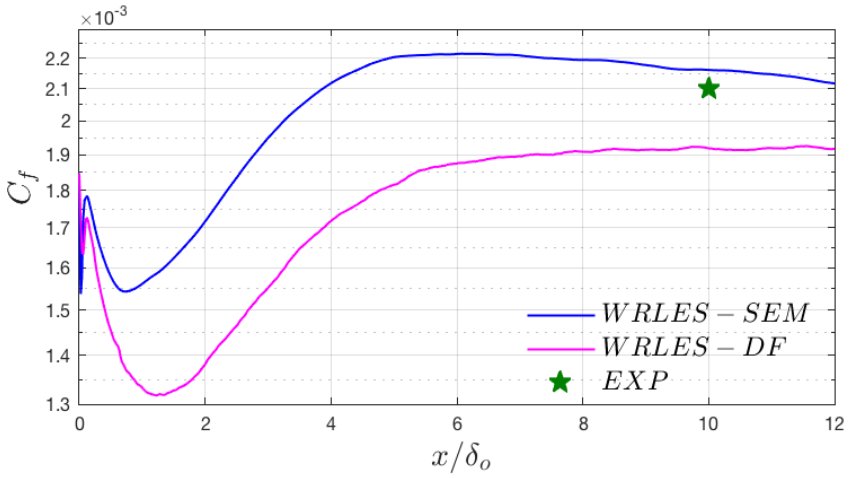

Figure 12.—Skin friction coefficient, for the comparison between WRLES-SEM and WRLES-DF.

5.3 Code-to-Code Comparison of Digital Filtering: WRLES-DF and FDL3DI-DF

The purpose of this subsection is to investigate sensitivities that may arise due to either the implementation and inputs of DF or the flow solver itself. In both WRLES-DF and FDL3DI-DF, the digital filter's integral length scale was set to be $\delta/2$ in all three directions (Ref. 15). The mean velocity profiles in wall coordinates at $x/\delta = 10$ are shown in Figure 13. The scaled mean velocities predicted by WRLES-DF and FDL3DI-DF are higher than the experiment.

Figure 14 shows the Reynolds stress profiles for the WRLES-DF and FDL3DI-DF, the solutions agree with experimental data especially in the outer portions of the boundary layer. Both the shear stress and streamwise stress are matched well and the peak is well predicted. The difference between both solutions although small is still observable. WRLES-DF consistently predicted higher peak values than FDL3DI. For instance, the peak shear stress is 0.93, 0.88, and 0.74 for WRLES-DF, FDL3DI-DF, and experiment respectively. Likewise, the peak streamwise stress is 9.5, 9.5, and 8.5 for WRLES-DF, FDL3DI-DF, and experiment respectively. Consistent with previous findings, Likewise, the peak streamwise stress is 1.3, 1.28, and 0.80 for WRLES-DF, FDL3DI-DF, and experiment respectively. The predicted peak value of spanwise stress is 2.6 (WRLES-DF) and 2.3 (FDL3DI-DF).

In Figure 15, the skin friction coefficient is shown. The value of both solvers match closely at 1.88E-3 and 1.92E-3 for FDL3DI-DF and WRLES-DF, respectively. Recall the experimental value is at 2.10E-3. Table 3 is a summary of all the cases examined. The adjustment length is 6δ for both WRLES-DF and FDL3DI-DF. The computational time between FDL3DI-DF and WRLES-DF are similar. The outcome of this comparison between two flow solvers is that both WRLES-DF and FDL3DI-DF reasonably agree on the value of C_f and Reynolds stress profiles, while providing good agreement with experiment.

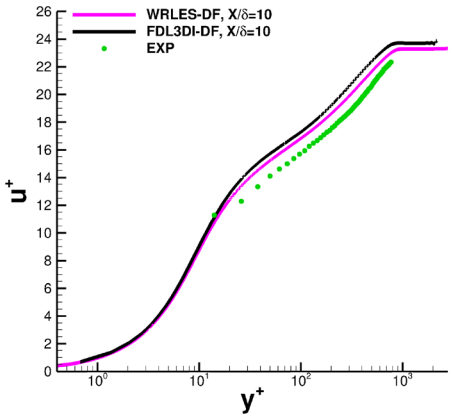

Figure 13.—Time averaged streamwise velocity, for the comparison between WRLES-DF and FDL3DI-DF.

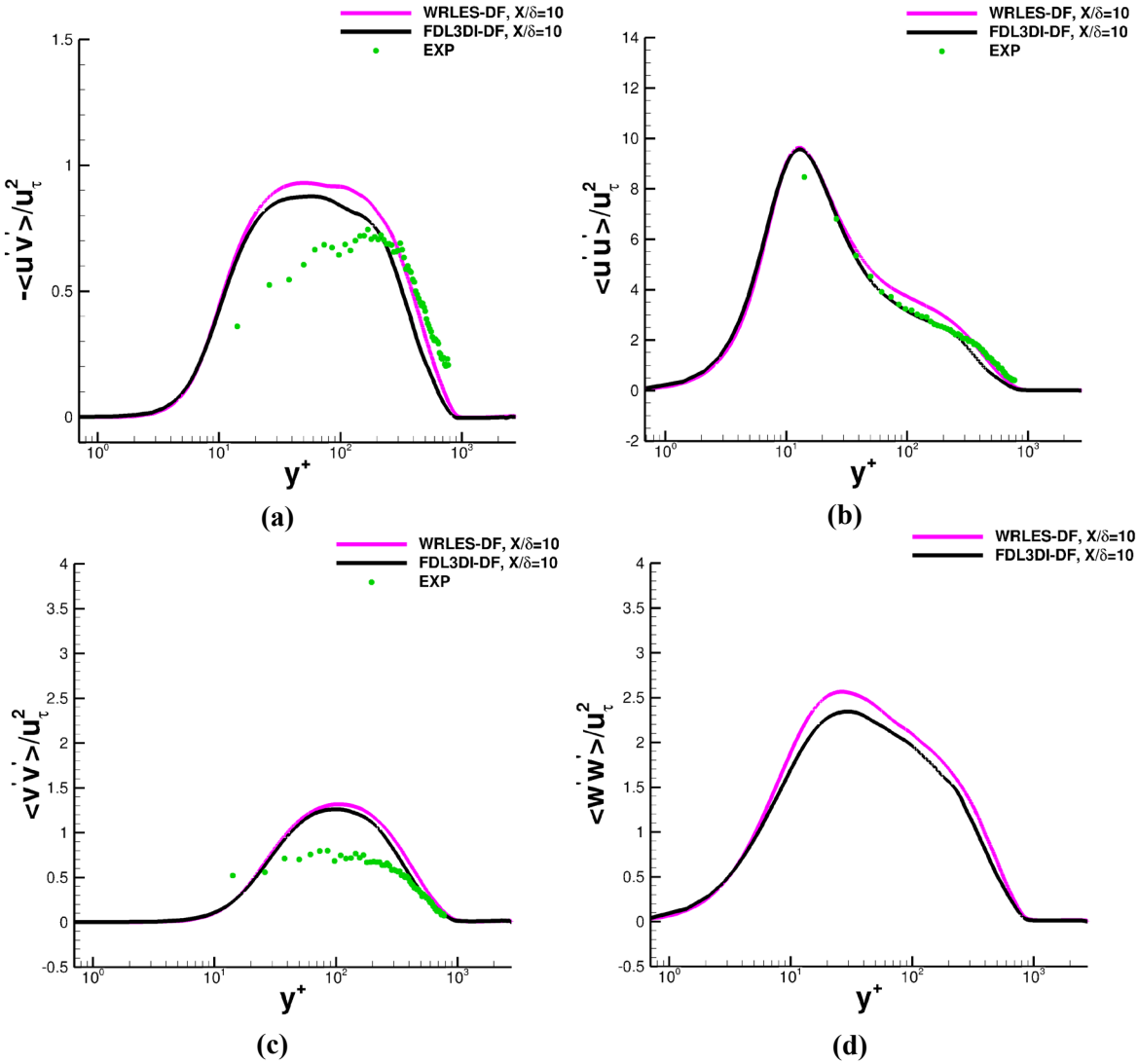

Figure 14.—Reynolds stresses: (a) shear stress; normal stresses (b) streamwise, (c) transverse, and (d) spanwise, for the comparison between WRLES-DF and FDL3DI-DF.

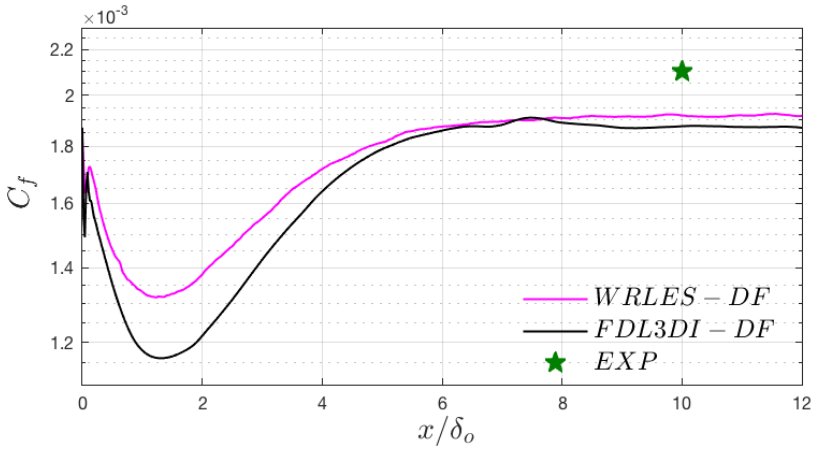

Figure 15.—Skin friction coefficient, for the comparison between WRLES-DF and FDL3DI-DF

6.0 Conclusions

Wall-resolved Implicit Large-eddy simulations were performed for a supersonic boundary layer to evaluate inflow turbulence methodologies. The first contribution of this work is a length scale study for the Synthetic Eddy Method (SEM) documenting its effects on the inflow spectra, downstream sustained Reynolds tensor, and C_f. The input normal stresses do not satisfy the LES equations. Hence an adjustment region downstream of the inflow, where the *synthetic* turbulence gives rise to *physical* turbulence. The skin friction coefficient was found to be a good descriptor of the adjustment region. The adjustment length was found to be unaffected by the SEM length scale. SEM imposes an artificial mode at the inflow plane that quickly vanishes. A small length scale attenuated the Reynolds stress profiles. In contrast, a large length scale resulted in the closest match between simulation and experiment for both the Reynolds stress profiles and the predicted skin friction coefficient. The turbulent spectra plots showed that large length scales resulted in more energy at lower frequencies, whereas small length scales resulted in energy at the higher frequencies, where it was dissipated. The adjustment length did not vary with SEM length scale and was discerned to be 6δ.

The second major contribution of this work is a comparison of two approaches within the WRLES code: (1) the Synthetic Eddy method; (2) the Digital Filtering (DF) method. A comparison with the experimental Reynolds stress data 10 boundary layer heights downstream of the inflow was used to validate the methods. The simulated values were in good agreement with the experimental values. Although digital filtering Reynolds stress predictions matched the experiment closely in the outer portions of the boundary layer, it predicted a 9 percent lower C_f value than experiment. The SEM $L = \delta/5$ case accurately predicted the 2.1E-3 C_f value of the experiment. Despite the differences between SEM and DF, both methods provided adequate inflow turbulence to the boundary layer and had the same adjustment length of 6δ. One method is not more robust than the other. The third contribution of this work is a comparison between two different flow solvers using Digital Filtering. The predictions made by both FDL3DI and WRLES are comparable. Both simulations predicted almost the same skin friction coefficient and had the same adjustment length.

The significance of this overall work is that both methods, Synthetic Eddy Method and Digital Filtering, accurately replicate the supersonic boundary layer after a finite adjustment length. This study points to the importance of investigating the downstream behavior of synthetic inflow turbulence. In particular, it points to the possibility of having the Reynolds stress profiles accurately replicated but still have a noticeable variation in skin-friction. The scaled mean flow profiles, Reynolds stresses, skin-friction coefficient, and dC_f/dx were comprehensively used to discern the adjustment length. The DF and SEM adjustment lengths were all 6δ.

References

1. Klein, M., Sadiki, A., Janicka, J., "A digital filter based generation of inflow data for spatially developing direct numerical or large eddy simulations." Journal of Computational Physics, 186, 652–665, 2003.
2. Lund, T., Wu, X., Squires, D., "Generation of turbulent inflow data for spatially-developing boundary layer simulations." *Journal of Computational Physics* 140, 233–258, 1998.
3. Di Mare, L., Klein, M., Jones, W. P., Janicka, J., "Synthetic turbulence inflow conditions for large-eddy simulation." *Physics* of Fluids, Vol. 18, 2006.
4. Mankbadi, M.R., DeBonis, J.R., Georgiadis, N.J., "Large-Eddy Simulation of a Compressible Mixing Layer and the Significance of Inflow Turbulence." AIAA Paper 2017-0316, 2017.
5. Mankbadi, M.R., Georgiadis, N.J., DeBonis, J.R., "Comparison of High-Order and Low-Order Methods for Large-Eddy Simulation of a Compressible Shear Layer." 45th AIAA Fluid Dynamics Conference, AIAA Aviation, 2015–2939.
6. Rana, Z., Thornber, B., Drikakis, D., "On the importance of generating accurate turbulent boundary condition for unsteady simulations." *Journal of Turbulence*, Vol. 12, No. 35, 2011.
7. Kempf, A., Klein, M., Janicka, J., "Efficient generation of initial- and inflow-conditions for transient turbulent flows in arbitrary geometries." *Flow Turbulence and Combustion*, Vol. 74, 2005.
8. Touber, E., Sandham, N., "Large-eddy simulation of low-frequency unsteadiness in a turbulent shock-induced separation bubble." *Theoretical and Computational Fluid Dynamics*, Vol. 23, 2009.
9. Morgan, B., Larsson, J., Kawai, S., Lele, S., "Improving low-frequency characteristics of recycling/rescaling inflow turbulence generation." *AIAA Journal*, Vol. 49, No. 3, March 2011.
10. Keating, A., Piomelli, U., Balaras, E., Kaltenbach, H., "A priori and a posteriori tests of inflow conditions for large-eddy simulation." *Physics of Fluids,* Vol. 16, No. 4696, 2004.
11. Xie, Z., Castro, I., "Efficient generation of inflow conditions for large eddy simulation of street-scale flows." *Flow Turbulence and Combustion*, Vol. 81, 2008.
12. Jarrin, N., Benhamadouche, S., Laurence, D., Prosser, R. "A synthetic-eddy-method for generating inflow conditions for large-eddy simulations." *International Journal of Heat and Fluid Flow*, 27(4), 585–593, 2006.
13. Jarrin, N., Prosser, R., Uribe, J.-C., Benhamadouche, S., Laurence, D., "Reconstruction of Turbulent Fluctuations for Hybrid RANS/LES Simulations using a Synthetic-Eddy Method." *International Journal of Heat and Fluid Flow*, Vol. 30, pp. 435–442, 2009.
14. Dussauge, J.P., Debieve, J.F., Dupont, P., Piponniau, S., Souverein, L.J., "Final Report on the Measurements of Shock Reflection at M = 2.25." UFAST, IUSTI Deliverable No. 3.3.5, 2009.
15. Vyas, V.A., Yoder, D.A., Gaitonde, D.V., "Reynolds-stress Budgets in an Impinging Shock Wave/Boundary-layer Interaction," AIAA Paper 2018-1299, 2018.
16. DeBonis, J.R., "A High-Resolution Capability for Large-Eddy Simulation of Jet Flows." AIAA Paper 2010-5023, 2010.
17. DeBonis, J.R., "Solutions of the Taylor-Green Vortex Problem Using High-Resolution Explicit Finite Difference Methods." AIAA Paper 2013-0382, 2013.
18. Bogey, C., Bailly, C., "A Family of Low Dispersive and Low Dissipative Explicit Schemes for Flow and Noise Computations." *Journal of Computational Physics*, Vol. 194, pp. 194–214, 2004.
19. Berland, J., Bogey, C., Bailly, C., "Low-Dissipation and Low-Dispersion Fourth-Order Runge–Kutta Algorithm." *Computers and Fluids*, Vol. 35, pp. 1459–1463, 2006.
20. Rizzetta, D.P., Visbal, M.R., Stanek, M.J, "Numerical Investigation of Synthetic-Jet Flowfields." *AIAA J.*, Vol. 37, pp. 919–927, 1999.
21. Visbal, M.R., Gaitonde, D.V., "On the Use of High-order Finite-difference Schemes on Curvilinear and Deforming Meshes." *Journal of Computational Physics,* Vol. 181, pp. 155–185, 2002.

22. Visbal, M.R., Rizzetta, D.P., "Large-Eddy Simulation on Curvilinear Grids Using Compact Differencing and Filtering Schemes." *Journal of Fluids Engineering,* Vol. 124, pp. 836–847, 2002.
23. Gaitonde, D.V., Visbal, M.R., "High-Order Schemes for Navier-Stokes Equations: Algorithm and Implementation into FDL3DI." Air Force Research Laboratory Tech. Rep. TR-1998-3060, Wright-Patterson Air Force Base, Ohio, 1998.
24. Georgiadis, N., Rizzetta, D., Fureby, C., "Large-Eddy Simulation: Current Capabilities, Recommended Practices, and Future Research." 47th AIAA Aerospace Sciences Meeting including The New Horizons Forum and Aerospace Exposition, 2009-948, 2009.
25. Georgiadis, N. J., Alexander, J. I. D., Reshotko E., "Hybrid Reynolds-Averaged Navier–Stokes/Large-Eddy Simulations of Supersonic Turbulent Mixing." *AIAA Journal*, Vol. 41, pp. 218–229, 2003.